

**Please cite the Published Version**

Huo, Shuan, Hemida, Hassan and Sterling, Mark  (2020) Numerical study of debris flight in a tornado-like vortex. Journal of Fluids and Structures, 99. 103134 ISSN 0889-9746

**DOI:** <https://doi.org/10.1016/j.jfluidstructs.2020.103134>

**Publisher:** Elsevier BV

**Version:** Accepted Version

**Downloaded from:** <https://e-space.mmu.ac.uk/634398/>

**Usage rights:**  Creative Commons: Attribution-Noncommercial-No Derivative Works 4.0

**Additional Information:** © 2020. This manuscript version is made available under the CC-BY-NC-ND 4.0 license <https://creativecommons.org/licenses/by-nc-nd/4.0/>

**Enquiries:**

If you have questions about this document, contact [openresearch@mmu.ac.uk](mailto:openresearch@mmu.ac.uk). Please include the URL of the record in e-space. If you believe that your, or a third party's rights have been compromised through this document please see our Take Down policy (available from <https://www.mmu.ac.uk/library/using-the-library/policies-and-guidelines>)

# Numerical Study of Debris Flight in a Tornado-like Vortex

Shuan Huo<sup>\*1)</sup>, Hassan Hemida<sup>2)</sup>, Mark Sterling<sup>3)</sup>

*Department of Civil Engineering, School of Engineering, University of Birmingham, Birmingham,  
United Kingdom*

*\*1) srh629@bham.ac.uk*

*2) h.hemida@bham.ac.uk*

*3) m.sterling@bham.ac.uk*

## Abstract

This paper presents the numerical study on the flight behaviour of spherical compact debris in a tornado-like wind field. The tornado-like vortex corresponding to a swirl ratio of 0.7 was generated using Large-eddy Simulation and the trajectories of 2250 individual debris particles placed in the flow were computed using Lagrangian-particle tracking. The debris corresponded to five groups (A, B1, B2, B3 and C) based on the value of the Tachikawa number ( $K$ ) which ranged between 0.6 and 2.5. An analysis of the simulated flow field revealed that the tornado-like vortex consisted of two main features - a core at the centre with low velocity ( $\sim 0.25\text{m/s}$ ) which was surrounded by thick vortex wall composed of high velocity magnitudes ( $\sim 9.4\text{m/s}$ ). Updraft flows were observed around the core of the vortex and as a result, debris positioned around the core radius region were found to be 24% more likely to become wind-borne than debris positioned at the vortex wall region. Three groups of debris (B1, B2 and B3) with varying mass and density were studied for the aerodynamic similarity by retaining the fixed value of  $K=1.2$ ; all three debris groups exhibited the propensity to travel with similar flight characteristics. An analysis of the data pertaining to the flight behaviour of the three debris group (A, B1 and C) with varying  $K$  revealed that the low mass debris group A ( $K=2.5$ ) had the highest propensity to become wind-borne and was more likely to travel for the longest time with considerable variability observed in individual debris trajectories. However, somewhat counterintuitively, the high mass debris group C ( $K=0.6$ ) were found to have the furthest impact range despite their short flight duration; this was due the high mass debris being ejected out of the vortex with greater inertia, while debris with a lower mass had a tendency to be trapped in the flow that circulates around the vortex core.

## 1. INTRODUCTION

Tornadoes are perhaps one of the most destructive weather phenomena due to their potentially violent and unpredictability nature. The wind speeds of a tornado can reach up to 450 kilometres per hour and can cause severe damage to civil structures and loss of lives. In March 2019, a tornado struck the Lee County in Alabama (USA) and caused catastrophic damage around the region: it was reported that the tornado was classed as an EF4 with wind speeds reaching 270 kilometres per hour (Darrow, 2019) and claimed the lives of more than 23 people. Tornadoes are complex phenomena and despite their frequent occurrence, surprisingly little is known about the flow structure. Due to the violent nature and unpredictable path of tornadoes, details of the tornado flow field using full scaled methods have, to date, proved to be rather elusive; therefore, recourse is often made through physical and numerical modelling. The earliest systematic experiment for generating laboratory-scaled tornado-like vortices can perhaps be attributed to Ward (1972). Ward developed a laboratory simulator with an exhaust fan at the top to provide updraft flow and vanes at the ground to generate angular momentum. This approach enabled the reproduction of tornado-like flow from a single-celled vortex

into a multi-celled vortex and provided an alternative to study tornado flows. However, Ward's simulators were limited by their size unable to reproduce some vortex characteristics due to the design. Therefore, an increasing number of studies have been conducted in order to numerically simulate such flow.

Recent numerical studies have been conducted extensively to study the flow fields of tornado-like vortices. Howells et al. (1988) and Nolan and Farrell (1999) used the axisymmetric Navier-Stokes equations in cylindrical coordinates to examine the flow structure of a tornado-like vortex. Lewellen et al. (1999) conducted Large-eddy Simulation (LES) to examine the interaction between the generated vortex and the surface roughness. Unsteady Reynolds-Averaged Navier-Stokes (URANS) model for the numerical simulation were performed by Hangan and Kim (2006) to reproduce tornado-like vortices. They concluded that the core of the tornado was the most difficult region to properly reproduce. Lewellen and Lewellen (2007) employed a LES turbulence model to study the effects of swirl ratio (a parameter which measures the strength of a circulation relative to the updraft flow) on vortex structure and translation speed. Kuai et al. (2008) conducted numerical research on full scale and laboratory simulated tornadoes using the k- $\epsilon$  turbulence model and verified the ability of numerical methods to capture the flow fields of the tornadoes. Hangan and Kim (2008) conducted simulations using an URANS model to reproduce tornadoes at different swirl ratios, and discovered that a high swirl ratio corresponded with full scale data from the Spencer tornado observed by Alexander and Wurman (2005). Ishihara et al. (2011) compared the flow fields of two different types of vortices and validated the results with the laboratory experiments. Natarajan (2011) numerically simulated different stages of tornadoes and confirmed the findings from earlier physical simulations is the primary governing parameter of a vortex. Research undertaken by Ishihara and Liu (2014) conducted an in-depth study of a tornado-like vortex during touch down stage with detailed analysis of the flow field; while Liu and Ishihara (2015) further investigated the stages of tornado-like vortices in order to capture of characteristics of the evolution of different vortex stage. The excellent research conducted by the aforementioned researchers and others provides an insight to tornado flows and its mechanism; however, the definition of the swirl ratio from these studies varies from one to another, therefore, detailed discussions on the definition of swirl ratio employed in this study were discussed in section 2.2.

Another key factor that contributes to the tornado induced damage is flying debris. Everyday objects can become damaging projectiles when subject to a tornado, and individuals have been affected considerably by debris which become windborne as a result of a tornado (Harms, 2019). Numerous research on flying debris have been undertaken since the pioneering works of Tachikawa (1983), which proposed a dimensionless parameter,  $K$ , which describes the ratio between the inertial forces of the flow to the weight of the debris. Wills et al. (2002) categorized debris based on their respective damage performance with light, medium or heavy weight missiles; other identification based on the geometrical structure can further categorize the debris into compact type (3D), plate type (2D) and rod type (1D). Further work on the trajectories of compact type (3D) spherical debris in strong winds was conducted by Holmes (2004) and English (2005). Baker (2007) also generalized the equations of motion for debris flight in dimensionless form for compact and sheet-like debris. Furthermore, plate-like (2D) debris (Tachikawa, 1983; Wang and Letchford, 2003; Holmes et al., 2004) and rod-like (1D) debris (Lin et al., 2007; Richards et al., 2008) under different wind conditions have also been studied extensively, but none of these studies were carried out under tornado-like flow conditions. Recently, several investigations on debris flight in tornadoes have been conducted; Maruyama (2011) simulated a tornado-like vortex using large eddy simulations with the statistical distribution of debris velocities. Bourriez et al. (2017) studied the flight paths of debris in laboratory controlled conditions. Research undertaken by Baker and Sterling (2017) provided an analytical model for the velocity and pressure

fields of tornadoes as well as the prediction of debris trajectories within the tornado. While these studies provide a great insight to the flow fields and trajectories, there is a lack of detailed analysis on flying debris in tornadoes. Hence, the objective of the present work was to investigate the behaviour of flying debris in a tornado-like wind field. The tornado-like vortex was simulated using LES. The flow fields of the vortex were analysed and the characteristics features were presented. Trajectories of five debris groups with varying Tachikawa number were computed and the flight data were analysed.

The paper is organized as follows: Section 2 describes the procedure adopted and the numerical details relating to this. Section 3 outlines the three dimensional flow field, characteristics and mechanisms of the simulated tornado-like vortex. The detailed analysis of debris flight in tornado wind field were discussed in section 4. Appropriate conclusions are given in section 5.

## 2. METHODOLOGY

### 2.1 DESCRIPTION OF PHYSICAL SIMULATOR

The model used in the current research was based on the University of Birmingham Tornado Vortex Generator (UoB-TVG), shown in figure 1. A series of physical simulations were undertaken by Gillmeier et al. (2017) and were used as validation for the numerical flow field simulated in the current paper. The UoB-TVG was a large-scale Ward-type vortex generator based on the design of Ward's simulator (Ward, 1972) with exhaust fans placed at the top of the convection chamber that were used to generate an updraft flow. Situated below the convection chamber was the convergence chamber, designed to draw air inwards with a series of guide vanes mounted at the edge of convergence chamber. Angular momentum was obtained by setting the guide vanes to different angles, thus generating different vortex structures. The convection chamber has the height,  $h_1$  of 2m and diameter,  $D_1$  of 3.1m and convergence chamber with the height,  $h_2$  of 1m and diameter,  $D_2$  of 3.6m with thirty guide vanes mounted around the edges of the convergence chamber. An exhaust outlet with diameter,  $D_3$  of 1m was situated at the top of the convection chamber. The ratio between updraft diameter and the height of the convergence chamber was defined as the aspect ratio,  $a$ . The velocity at the inlet ( $U_\infty$ ) was 0.66m/s, which was computed based on the measured total outflow rate ( $Q$ ) of 7.38 m<sup>3</sup>/s at the exhaust outlet. The velocity measurements of the flow field were made 100Hz using the Cobra Probe (Watkins et al., 2002) which was mounted in the simulator.

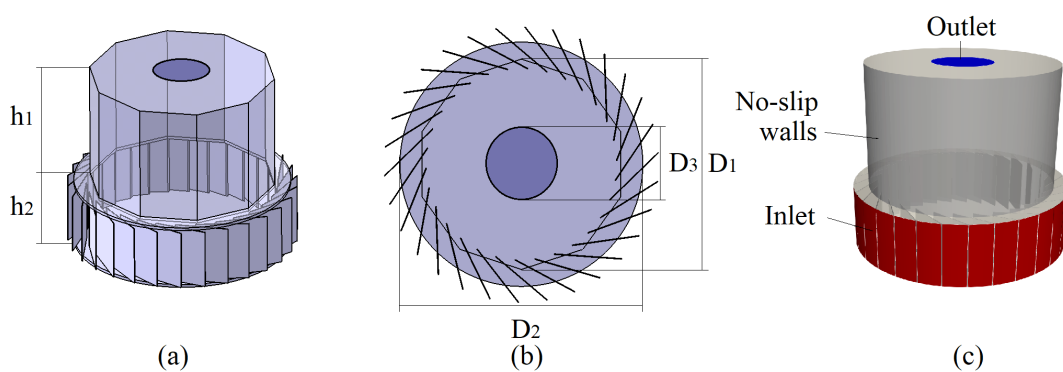


Figure 1: (a) Geometry of the University of Birmingham Tornado Vortex Generator (b) Dimensions of the convergence chamber (c) Computational domain and boundary conditions.

### 2.2 SWIRL RATIO

Whilst there are some variations for the definitions of swirl ratio in most laboratory studies (Monji, 1985, Mishra et al., 2008, Matsui and Tamura, 2009, Tari et al., 2010 and Gillmeier et al., 2017) and numerical studies (Wilson and Rotunno, 1986, and Ishihara et al., 2011 and Ishihara and Liu, 2014),

the swirl ratio has generally been defined as the measure of intensity of the circulation of a vortex, while also describing the evolution of the stages of a tornado; from single-celled to multi-celled vortex. The swirl ratio,  $S$  used in the current research has been defined as:

$$S = \frac{\tan\theta}{2a} \quad [1]$$

where  $\theta$  is the guide vanes angles and  $a$  is the aspect ratio, defined as:

$$a = \frac{2h_2}{D_3} \quad [2]$$

The definition of the aspect ratio is based on the physical dimensions of the simulator; the ratio between the diameter of the exhaust outlet ( $D_3$ ) and the height of the inlet ( $h_2$ ). The UoB-TVG has a fixed aspect ratio of 2, while other large-scale tornado vortex simulators have adjustable aspect ratios such as the WindEEE dome (Refan and Hangan, 2018) with aspect ratio of 0.35 to 1, VorTECH (Tang et al., 2017) of 0.5 to 1 and ISU Tornado simulator (Gairola and Bitsuamlak, 2019) of 1.09 to 5.46.

## 2.3 NUMERICAL DETAILS

The Large-eddy simulation approach employed in the current research was first proposed by Smagorinsky (1963); the LES uses sufficiently small grid resolution to directly compute the larger eddies in a turbulent flow, while the smaller unresolved scales of the turbulence were filtered and modelled via the sub-grid scale (SGS). Studies by Natarajan (2011), Maruyama (2011), Ishihara et al. (2011) and Ishihara and Liu (2014) found that the vortex core contains complicated turbulent flows and thus ideally suited to an LES. The open source CFD program OpenFOAM (OpenFOAM, 2019) was used to perform the LES with the assumption that the flow was incompressible and Newtonian in nature. The continuity and momentum equations were filtered as follows in order to obtain the governing equations:

$$\frac{\partial \bar{U}_i}{\partial x_i} = 0 \quad [3]$$

$$\frac{\partial \bar{U}_i}{\partial t} + \frac{\partial \bar{U}_i \bar{U}_j}{\partial x_j} = -\frac{\partial \bar{P}}{\partial x_i} + 2\frac{\partial}{\partial x_j}(v + v_{sgs})\bar{S}_{ij} \quad [4]$$

where  $U$  is the velocity field,  $t$  is the time and  $v$  is the kinematic viscosity. The spatial filtering operation for the LES is denoted by the bar over the physical quantities. The pressure ( $P$ ) and filtered strain rate tensor ( $\bar{S}_{ij}$ ) are expressed as:

$$\bar{P} = \frac{\bar{p}}{p} + \frac{(\bar{U}_i \bar{U}_j - \bar{U}_i \bar{U}_j)}{3} \quad [5]$$

$$\bar{S}_{ij} = \frac{1}{2} \left( \frac{\partial \bar{U}_j}{\partial x_i} + \frac{\partial \bar{U}_i}{\partial x_j} \right) \quad [6]$$

The Smagorinsky model (Smagorinsky, 1963), was used to model the eddy viscosity under the effects sub-grid scale,  $v_{sgs}$  with the eddy viscosity coefficient as:

$$v_{sgs} = (C_s f_d \Delta)^2 \sqrt{2 \bar{S}_{ij} \bar{S}_{ij}} \quad [7]$$

where  $f_d$  is the damping function,  $\Delta$  is the length scale of the SGS turbulence and  $C_s$  is the model coefficient, set to 0.1. The Van Driest type damping function (Van Driest, 1956) was employed in this study to calculate  $f_d$  and is expressed as:

$$f_d = 1 - \exp\left(\frac{-y^+}{25}\right) \quad [8]$$

where  $y^+$  is the non-dimensional distance to the wall, depicted as the relationship between friction velocity and kinematic viscosity.

## 2.4 COMPUTATIONAL DOMAIN AND BOUNDARY CONDITIONS

The computational domain was created based on the configurations of the UoB-TVG, which was geometrically similar to the study by Gillmeier et al. (2017) as illustrated in figure 1. The convection chamber was simplified to a cylinder configuration for the convenience of grid generation. A cartesian coordinate system has been adopted for the generation of the computational domain, where the  $xy$  plane represents the horizontal plane while  $z$  axis represents the axis perpendicular to the horizontal plane. The flow enters the convergence chamber with a uniform velocity of  $U_\infty=0.66$  m/s. The exhaust outlet was set with pressure outlet with the free stream pressure,  $P_\infty=0$ . A no-slip boundary condition was applied to the ground, surface walls of the guide vanes and the walls of the convection region. The results presented in this study were normalized using the characteristic parameters of the vortex: the maximum tangential velocity ( $U_T$ ), the radius of the core ( $r_c$ ) and time per revolution of the vortex ( $t_r$ ). The method of determining the location of maximum tangential velocity and the radius of the core are presented in section 3.2, while the time taken for the vortex to complete a single revolution is defined as:

$$t_r = \frac{2\pi r_T}{U_T} \quad [9]$$

where  $r_T$  is the radial distance of the maximum tangential velocity. The pressure coefficient,  $C_p$ , is a non-dimensional parameter defined as:

$$C_p = \frac{P - P_\infty}{0.5 \rho_a U_T^2} \quad [10]$$

and  $\rho_a$  is the density of the air. The simulation was initialised with the inlet velocity,  $U_\infty$ . A second order implicit backward scheme was used to approximate the time discretization. The gradients were discretized with the second order central differencing scheme and the implicit PISO solver was used. (OpenFOAM, 2019). A constant time-step of  $\Delta t= 5 \times 10^{-4}$  s was used throughout the entire transient simulation; this time-step was chosen to maintain the Courant-Friederichs-Lewy number (Courant et al., 1928) at the value less than 1 at every time step. The averaging of pressure and velocity were implemented when the vortex flow was fully developed, this was conducted by monitoring the residuals of each turbulent equation for convergence which ensured that the statistics did not change with time. Time time-averaged results were obtained by averaging the actual simulation time of 30 seconds, which is equivalent to 300 vortex revolutions.

## 2.5 MESHING

ICEM-CFD (ICEM, 2012) mesh generator package was used to generate quadrilateral structured mesh. In order to resolve the boundary layer around the viscous sub-layers, 20 layers of mesh were created with the wall-adjacent spatial unit of  $z^+=1$ . Due to the axisymmetric structure of the tornado-like vortex, a clustered mesh with high density was adopted at the centre of the convergence chamber within the radius of 0.6 m from the centre, resulting in  $x^+$  and  $y^+ \approx 10$  in the tangential and radial directions. Hyperbolic stretching was used to generate the remaining meshes to ensure smooth transition. The mesh resolution around the guide vane regions in the convergence chamber were adjusted for the generation of three different mesh resolutions - coarse, medium and fine mesh with 4 million, 7 million and 9 million cells respectively. The configuration of the generated mesh is shown in figure 2. Whilst every effort has been made to accurately reproduce the physical simulator there will inevitably be small differences introduced due to the meshing process. It is difficult to quantify the impact of these differences, but in what follows it is assumed that beyond a certain mesh resolution their effects are negligible (see section 3).

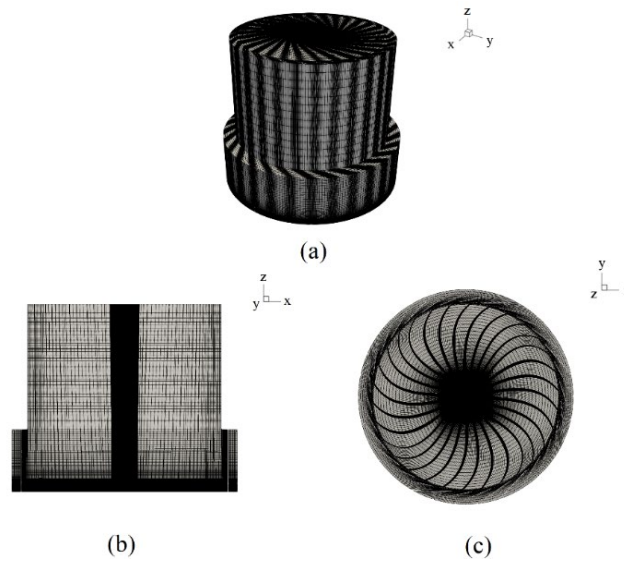


Figure 2: Mesh of the computational domain: (a) Isometric view (b) Side view (c) Top view.

## 2.6 COMPUTATION FOR FLYING DEBRIS

The three-dimensional motion of the debris in the tornado-like vortex was numerically computed. Each individual debris was assumed to be a three dimensional spherical compact object which did not undergo rotation. The Tachikawa number (Tachikawa, 1983) used in the current research is defined as:

$$K = \frac{\rho_a U_\infty^2 d^2}{2m_d g} \quad [11]$$

where  $\rho_a$  is the density of the air,  $U_\infty$  is the inlet velocity,  $d$  is the diameter of the debris,  $m_d$  is the mass of the debris and  $g$  is the acceleration due to gravity. The Tachikawa number  $K$ , describes the ratio between the aerodynamic forces to the gravitational force, therefore, debris with lower mass will have higher value of  $K$  and are in theory, prone to fly higher and further. Properties of the debris considered in the current study were shown in table 1.

Table 1: Properties of the debris groups

Debris group	$K$	Diameter (m)	Density (kg/m <sup>3</sup> )	Mass (kg)
A	2.5	0.00075	28.1	$6 \times 10^{-9}$
B1	1.2	0.0015	28.1	$50 \times 10^{-9}$
B2	1.2	0.00075	56.2	$12 \times 10^{-9}$
B3	1.2	0.00037	112.4	$3 \times 10^{-9}$
C	0.6	0.003	28.1	$397 \times 10^{-9}$

The trajectories of the debris were computed using the transient solver icoUncoupledKinematicParcelFoam (OpenFOAM, 2019), where the motion was solved by considering the particle equilibrium using the Lagrangian frame of reference on the established flow field. Since the size of the largest debris considered (debris group C) was  $\sim 10^8$  times smaller than the convergence chamber, the effects of debris on the flow were considered to be negligible. Hence, a one-way coupling was assumed to be sufficient, where debris were treated as point mass and generalized by:

$$\frac{ds_d}{dt} = U_d \quad [12]$$

$$m_d \frac{dU_d}{dt} = F_{total} \quad [13]$$

where  $s_d$  is the spatial position of the debris,  $U_d$  is the debris velocity, and  $F_{total}$  as the sum of all forces. The relevant forces acting on the particle were:

$$F_{total} = F_D + F_G \quad [14]$$

where  $F_D$  is the drag force and  $F_G$  is the gravitational force. These forces represent the dominant forces acting of the debris, while other forces were neglected. The drag force is expressed as:

$$F_D = \frac{3}{4} \frac{\rho_a m_d}{\rho_d d} \cdot C_D (U - U_d) |U - U_d| \quad [15]$$

where  $U$  is the velocity of the local flow field, and  $C_D$  is the spherical drag coefficient that is computed based on the debris Reynolds number (Putnam, 1961) as:

$$C_D = \begin{cases} \frac{24}{Re_d} (1 + \frac{1}{6} Re_d^{\frac{2}{3}}), & Re_d \leq 1000 \\ 0.424, & Re_d > 1000 \end{cases} \quad [16]$$

222

$$Re_d = \frac{\rho_a U d}{\mu_a} \quad [17]$$

where  $\mu_a$  is the viscosity of air. Each debris group was simulated for 50 time instances in the flow. At each time step, 9 debris were placed at different radial positions on the ground to be initialized by the flow, at 0m, 0.0275m, 0.55m, 0.0825m, 0.11m, 0.165m, 0.22m, 0.275m and 0.33m. A total of 2250 debris were released in the flow field.



### 3. RESULTS FOR THE TORNADO-LIKE VORTEX

#### 3.1. ASSESMENT OF NUMERICAL ACCURACY

In order to investigate the impact of grid resolution on the numerical results, computations were conducted on three mesh resolutions- coarse, medium and fine meshes. The velocity components  $U_t$ ,  $U_r$  and  $U_v$  represents the tangential, radial and vertical velocities respectively. Due to the axis-symmetrical structure of the vortex, horizontal positions from the centre were expressed using the radial distance,  $r$ . Figure 3 shows the comparison of vertical distribution of time averaged tangential velocity extracted from different locations,  $r=0.1, 0.15, 0.2$  and  $0.25\text{m}$ . At all radial positions, the coarse, medium and fine meshes show similar trends with respect to the vertical distribution of the tangential velocity, with the medium and fine meshes both predicted similar results. The maximum tangential velocities obtained from the three meshes are 11.7, 12.4 and 12.5 m/s for coarse, medium and fine meshes, respectively.

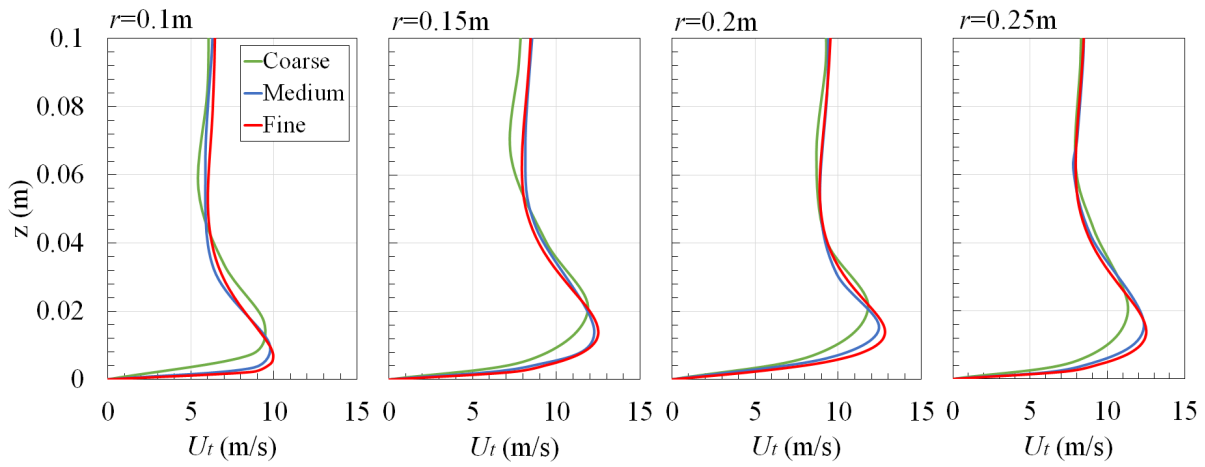


Figure 3: Vertical profiles of time averaged tangential velocity at the position  $r/r_c = 1, 1.5, 2$  and  $2.5$ .

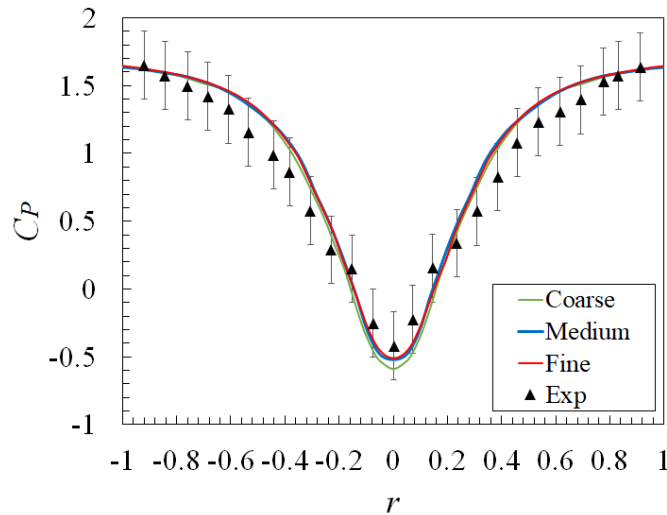


Figure 4: Distribution of time averaged pressure coefficient on the ground surface in comparison with experimental data Gillmeier et al. (2017).

The experimental results of Gillmeier et al. (2017) were used as a comparison for the numerical simulation. It is worth noting that experimental velocity and pressure data have an uncertainty of  $\pm 2\%$  and  $\pm 0.5\%$ . Figure 4 illustrates the agreement between the numerical simulations and experimental data in terms of surface pressure coefficient. For all meshes it can be observed that the

data from LES agrees well in terms of magnitude and trend with the experimental data. (A comparison using the velocity measurements is presented later in section 3.2 and shows a similar level of agreement with the medium mesh.)

### 3.2 FLOW FIELD

The results from the numerical simulation of a tornado-like vortex with the swirl ratio of 0.7 are presented in this section. The flow features of the vortex structure were analysed and the method of determining the radius of the core and vortex wall thickness are discussed. Figure 5 illustrates the contours of instantaneous velocity magnitude and the vectors of averaged radial and vertical velocity, where  $U_{mag}$  denotes the velocity magnitude of the flow field. The tornado-like vortex consists of two main features, a vortex core and thick vortex walls. The core is situated at the centre of the vortex while the wall surrounds the core and gives an outline to the structure of the vortex. The vortex was observed to exhibit a very minor and random wandering motion where the core shifts at the maximum distance of approximately  $r/r_c=0.18$  from the centre axis. Based on the velocity vectors, the centre of the vortex consists of downwards flow - a region of inflow was observed towards the centre, and then redirects towards the vertical direction. The radial distance in which separates the upwards and downwards flow was identified as the core radius.

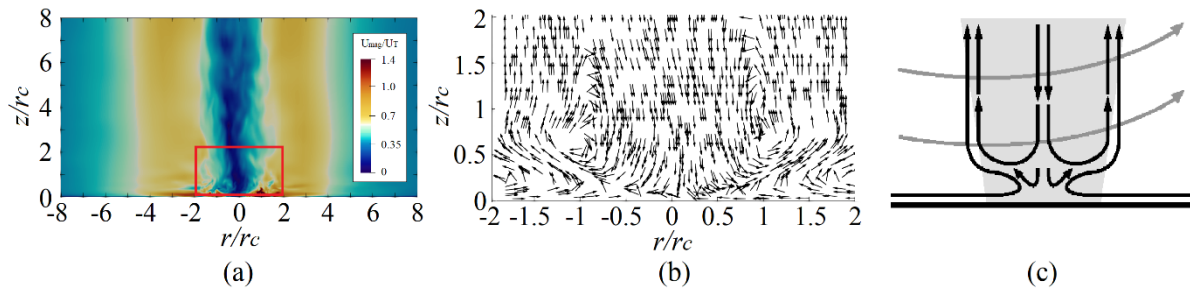


Figure 5: (a) Contours of instantaneous velocity magnitude of tornado-like vortex (b) Averaged radial and vertical velocity vector of the regions in the red box (c) Sketch of the tornado-like vortex to illustrate the flow structure.

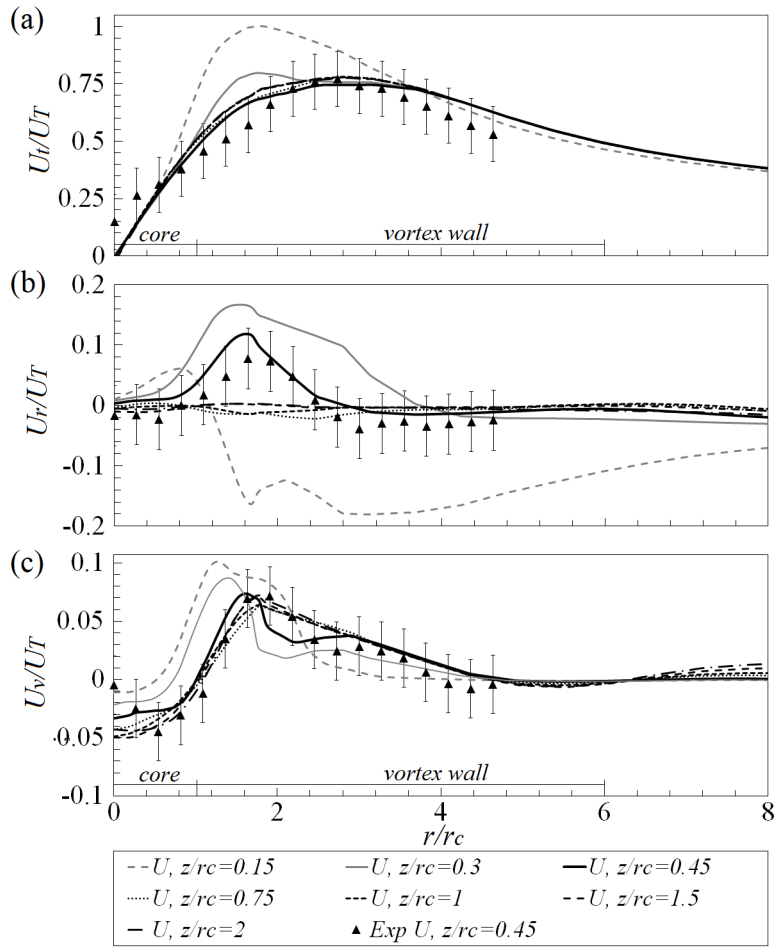


Figure 6: Horizontal profiles of time averaged velocity components at different elevation in comparison with experimental results (Exp) by Gillmeier et al. (2017).

Figure 6 shows the horizontal profiles of time averaged velocities extracted from the flow fields at the elevations of  $z/r_c=0.15, 0.3, 0.45, 0.75, 1, 1.5$  and  $2$ . The experimental results by Gillmeier et al. (2017) were ensemble averages used as a comparison for the numerical simulation; data shown in the figure corresponds to the elevation of  $z/r_c=0.45$  (where  $r_c$  is the core radius). The maximum tangential velocity of the vortex,  $U_T$  was  $12.53$  m/s and occurs at the radial distance,  $r_T$  of  $1.82$  ( $r/r_c=1.82$ ) at the elevation of  $z/r_c=0.15$ ; the velocity  $U_T$  was used as a characteristic velocity, as shown in figure 6(a).

The time per revolution of the vortex,  $t_r$  was calculated based on  $r_T$  and  $U_T$ , revealing the vortex to be approximately  $0.1$  seconds per revolution. The normalised radius of the core ( $r/r_c=1$ , where  $r_c=0.11$ m) was calculated based on the averaged radial distance with respect to height of the layer with zero vertical velocity, ( $U_v/U_T=0$ ) (as shown in figure 6(c)). The tangential velocity at  $r_c$  was  $U_t/U_T=0.48$ , and was used to mark the boundaries of the vortex wall spanning from approximately  $r/r_c=1$  to  $6$  (as shown in figure 6(a)). As a result, the core at the centre of the vortex consists of low velocities, while high velocity magnitudes surround the core within the vortex wall.

In general, apart from the profile of  $z/r_c=0.15$ , the distribution of tangential velocity shows a similar trend and magnitude at all elevations. In figure 6(b), the profile at  $z/r_c=0.15$  shows an outwards flow from the centre of the vortex to the radial distance  $r/r_c=1.2$  and then changes to inflow as the radial distance increases. Low magnitudes of radial velocity components were observed at higher elevations. Based on the profiles of vertical velocities in figure 6(c), a similar distribution can be observed at all elevations, with negative velocities at the centre of the vortex and increasing to maximum magnitude

between  $r/r_c=1.5$  to  $1.8$ . Some minor differences can be observed around the core region between  $r/r_c=0$  to  $2$ , where the experimental results have the highest uncertainties. Overall, the predicted velocity field matches that given by the physical results. However, both the numerical and physical simulations are not without their limitations: accurately specifying inflow boundary conditions are crucial for LES yet fraught potentially with difficulties (Yang, 2015), as very specific information on turbulence is required to reproduce identical inflows, e.g., turbulence intensity, stochastically varying turbulent length scales, and power spectrums of turbulent etc. The effects of sub-grid scale (SGS) modelling is also considered to be a potential source of uncertainty since SGS motions inevitably requires unrealistically fine cells at all regions even locations far away from the vortex structure. Notwithstanding these limitations, the numerical results presented in the paper are within the range of experimental uncertainty and considered suitable for the purposes of this work.

## 4 RESULTS FOR DEBRIS FLIGHT

The results for the simulation of debris flight using the flow field outlined in section 3.2 are presented in this section. In all cases, the results have been normalized with the parameters of  $U_T$ ,  $r_c$  and  $t_r$  as appropriate. Debris group A, B1, B2, B3 and C (presented in table 1) were simulated at 50 different time instances respectively; the release times were chosen at every quarter revolution of the vortex, ( $t_r \approx 0.025s$ ). A total of 2250 individual debris groups were released from 9 different locations in the flow; 5 locations within the core of the vortex at  $r/r_c=0, 0.25, 0.5, 0.75$  and 4 locations away from the core at  $r/r_c=1.5, 2, 2.5$  and  $3$ . Results from the simulation of debris group B1, B2 and B3 with identical Tachikawa number of  $K=1.2$  were compared for the aerodynamic similarity in section 4.1, while section 4.2 investigates the behaviour of debris with varying Tachikawa number of  $K=2.5, 1.2$  and  $0.6$  for debris group A, B1 and C respectively.

### 4.1 RESULTS FOR DEBRIS B1, B2 AND B3 ( $K=1.2$ )

The distribution of flight duration of all released debris are shown in figure 7 and expressed in terms of the flight duration of each individual debris,  $t_d$ , normalized by the revolution of the vortex,  $t_r$ . The flight duration was calculated based on the total airtime of debris from initialization to the impact on the ground surface, where the maximum and minimum flight durations are represented by the whiskers on the box plots. It can be observed that all 3 debris types show similar interquartile range with positive skew; the mean flight duration (denoted by a "x") was approximately  $t_d/t_r \approx 4$  in all cases. Debris that were not initialized or had a flight duration of less than a single revolution, (i.e.,  $t_d/t_r < 1$ ) were not considered as wind-borne in the current analysis; as a result, the total number of wind-borne debris for debris group B1, B2 and B3 were 90, 82 and 86 respectively (20%, 18% and 19% for debris group B1, B2 and B3 respectively). The low percentage of windborne debris were not too surprising as this study focuses only on the wind-borne behaviour in a stationary tornado, where the translation effects of the tornado were ignored. However, it is worth noting that the translational movement of a naturally occurring tornado could potentially result in higher percentage of debris becoming wind-borne; several researches (Kosiba et al., 2014; Matsui et al., 2008; Phuc et al., 2012) have been carried out where the translating speed of tornado ranges from  $0.05 U_T$  to  $0.7 U_T$ .

Figure 8 illustrates the plan view of the trajectories of wind-borne debris for debris group B1, B2 and B3 that were initialized from the locations of  $r/r_c=0.5, 0.75, 1, 1.5$  and  $2$ . Data pertaining to the locations  $r/r_c=0, 0.25, 2.5$  and  $3$  are not shown since debris flight initialized from these locations was infrequent, largely due to the downwards flow at the centre of the vortex region ( $r/r_c=0$  and  $0.25$ ) and the absence of updraft flow at regions further from the core ( $r/r_c=2.5$  and  $3$ ). In general, the trajectories of all debris from group B show a very similar path distribution at all locations, although debris initialized from the location  $r/r_c=0.5$  tends to show a greater degree of variation in trajectory.

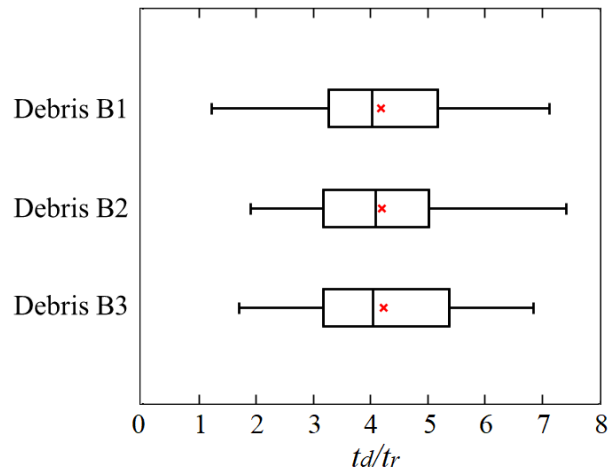


Figure 7: The distribution of flight duration of debris group B1, B2 and B3

The results from the experimental research conducted by Bourriez et al. (2017) were used as a comparison. The experimental study investigates the flight behaviour and motion of wind-borne debris in the tornado-like vortex at the swirl ratio of  $S=0.7$ . The debris used in the experiments were spherical polystyrene beads with varying diameter of 1.5 – 1.7 mm and densities of 24-28 kg/m<sup>3</sup>, and corresponds to debris group B1 used in the simulation. The motion of the debris were tracked using the 3D-PTV technique (Maas et al., 1993; Malik et al., 1993). Two high speed digital cameras (Sony NEX-FS700RH) were positioned in the simulator and setup to record videos at 480 fps with the resolution of 1920 x 1080 pixels (confines of the tracking window not specified). Variations in results were found due to the relatively inconsistent size of the debris used, and the considerable changes on the local field of the vortex due to the wandering motion or turbulent fluctuations. Figure 9 shows the comparison of debris trajectories from numerical simulation and experimental results. The locations of  $r/r_c=1$  and 2 corresponds to the closest release position from the experiments at  $r/r_c \approx 0.9$  (100mm) and  $r/r_c \approx 1.8$  (200mm).

The trajectories of the wind-borne debris were represented in black solid lines for the results from numerical simulation and the grey lines from the experiments while the red solid lines represents the mean trajectory of the numerical simulation and red dashed lines represents the mean trajectory of the experimental results.

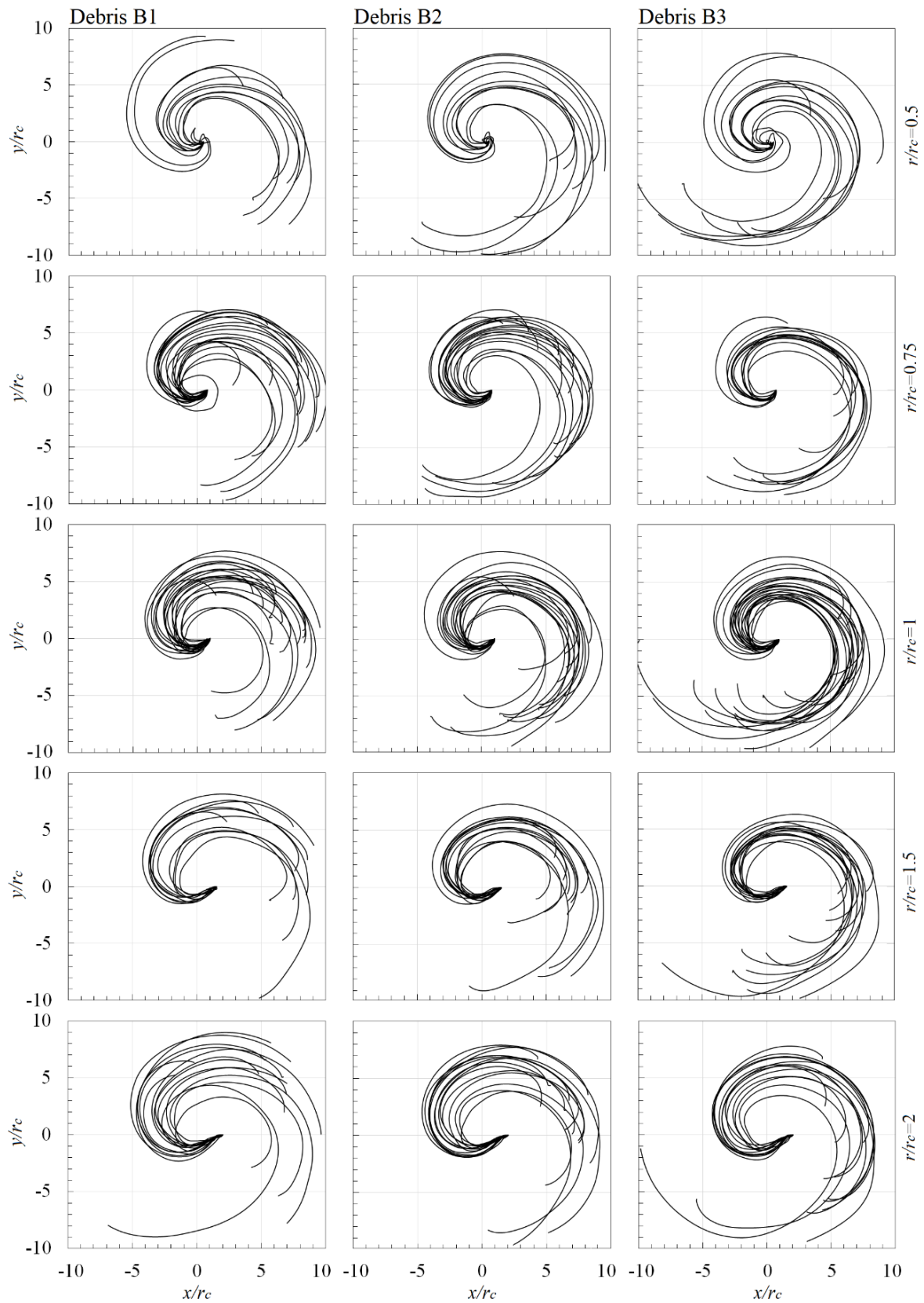


Figure 8: Plan view of debris trajectories at the locations of  $r/r_c=0.5$ , 0.75, 1, 1.5 and 2 for debris group B1, B2 and B3.

All three debris groups predicted similar distributions of debris trajectories at both release positions, while the debris trajectories from the experimental results shows shorter trajectories in comparison with the numerical simulation as debris left the tracking window and the entire trajectories were not captured. Both the numerical and experimental results corresponds well (considering the uncertainty associated with the results) at the location  $r/r_c=1$  with the overlapping trajectory path of approximately 78%; while at the location  $r/r_c=2$ , the overlapping region was lower at approximately 61%; the numerical simulation predicted trajectories that were closer to the vortex core while the experiment shows trajectories that were further from the core. The mean trajectories of both the experiments and numerical simulations shows very similar curvature with the distance of approximately  $r/r_c=0.4$  apart; this is likely due to the larger variation in the trajectory paths from the experiments, caused by the turbulent fluctuation in the local field.

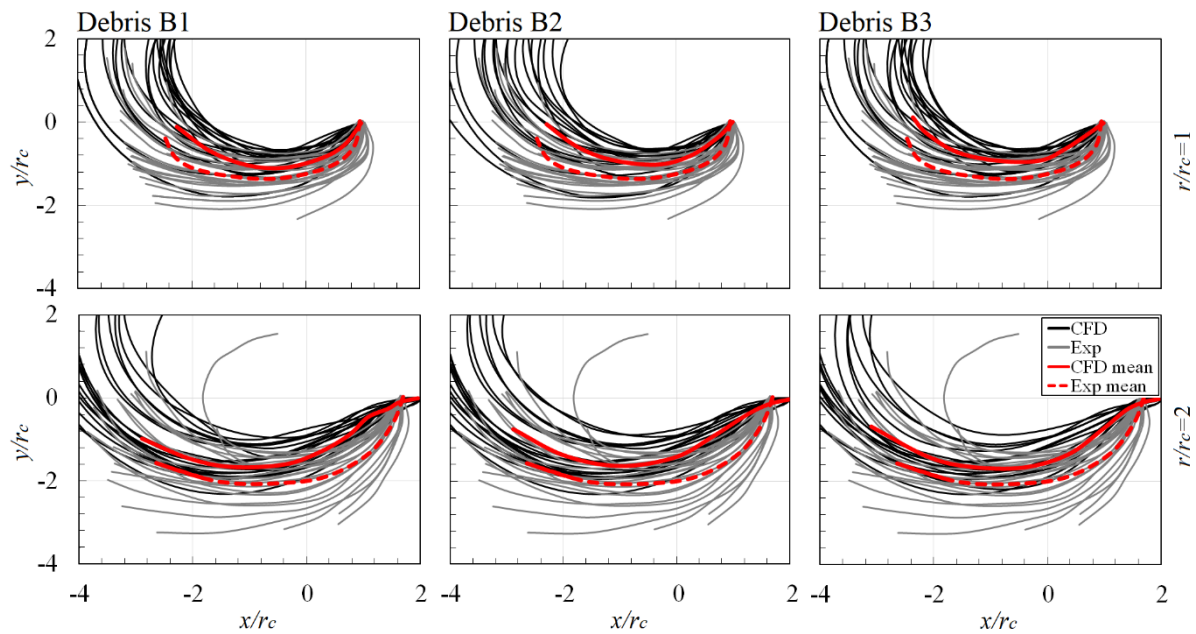


Figure 9: A close-up view of debris trajectories at the locations of  $r/r_c=1$  and 2 for debris group B1, B2 and B3 in comparison with experimental data from Bourriez et. al (2017).

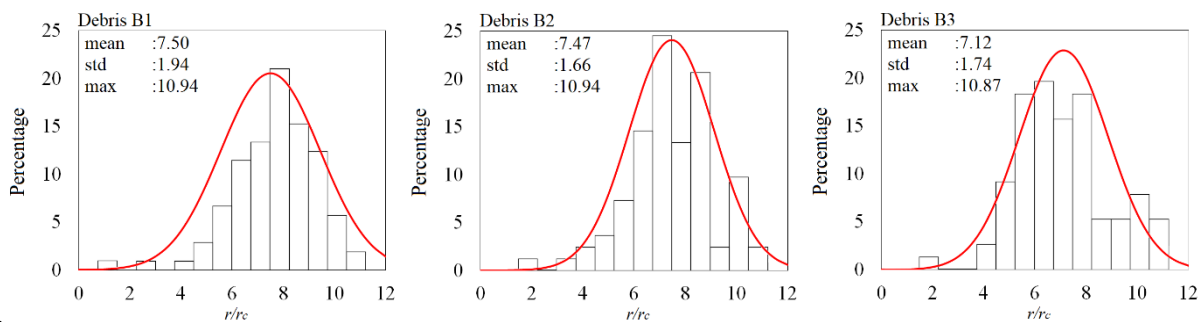


Figure 10: The distribution of impact radius of all released debris based on debris group, with mean, standard deviation and maximum values.

In figure 10, the bar chart shows the distribution of impact radius while the curve (red line) corresponds to the normal distribution of all wind-borne debris, expressed in terms of the percentage of occurrence against the impact radius. The distance between the impact locations and the centre of the vortex was expressed as the impact radius as this provides a measurement of damage range for the tornado-like vortex, while the percentage was calculated based on the number of occurrence for



wind-borne debris that impacts at that respective radial distance. The mean impact radius for debris group B1, B2, and B3 were 7.5, 7.5 and 7.1 respectively. Due to high magnitudes of velocity components between  $r/r_c=0$  to 3, a sparse distribution of debris impact was observed around that region. A clustered distribution of debris impact can be seen around the edge of the vortex walls that is further away from the core ( $r/r_c > 6$ ), where velocity magnitudes were low.

The aerodynamic similarity of debris group B1, B2 and B3 was examined. Understandably, all 3 debris groups were shown to exhibit the propensity to travel with very similar flight duration and trajectories due to the identical value of Tachikawa number. In general, the prediction of debris trajectories corresponds well for both the numerical simulation and experiments results; however, it should be pointed out that debris were assumed to be one-way coupled and the motion of debris were also assumed with no rotation in a highly swirling flow, which may result in some difference in overall trajectories between numerical and physical simulation. We also note the lack of turbulence data associated with the physical measurements results in an uncertainty of the flow simulation in this region. Notwithstanding this the numerical simulation are consistent with the physical data and able to capture the entire flight duration from initialization to the impact on the ground. Furthermore, the numerical simulations provide a better understanding of the impact distribution and extend the results of the physical simulation.

#### 4.2 RESULTS FOR DEBRIS A, B1 AND C ( $K = 2.5, 1.2$ AND $0.6$ RESPECTIVELY)

In this section, the behaviour of wind-borne debris in tornado-like vortex with varying Tachikawa number ( $0.6 - 2.5$ ) was studied. The distribution of flight duration for all released debris are shown in figure 11, expressed in terms of the flight duration of each individual debris,  $t_d$ , normalized by the revolution of the vortex,  $t_r$ . The flight duration was calculated based on the total airtime of debris from initialization to the impact on the ground surface, where the maximum and minimum flight durations are represented by the whiskers on the box plots. Debris that were not initialized or had a flight duration of less than a single revolution,  $t_d/t_r < 1$  were not considered as wind-borne. As a result, the total number of wind-borne debris for debris group A, B1 and C was 122, 90 and 54 respectively (27%, 20% and 12% for debris group A, B1 and C respectively). The Tachikawa number is a ratio of aerodynamic forces relative to gravitational force of a wind-borne debris, therefore, light debris (low mass) with high values of  $K$  will have the tendency to stay airborne for longer. Hence, the mean flight duration (red "x") for all 3 debris groups were considerably different; the smaller and lighter debris A has significantly longer flight duration than the heavier and larger debris C. The mean flight duration for debris group A, B1 and C were  $t_d/t_r = 5.49, 4.19$  and  $2.79$  respectively.

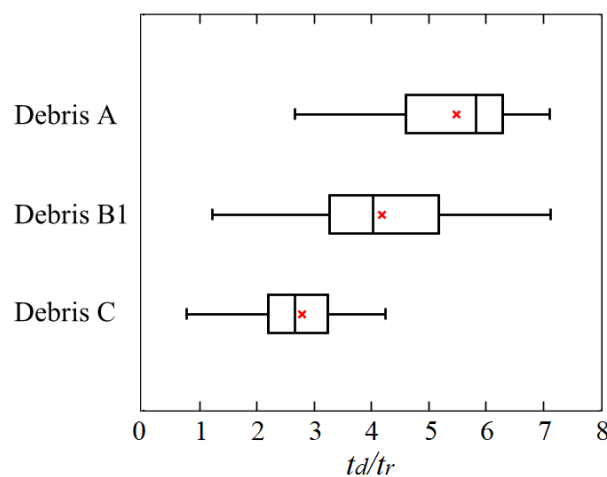


Figure 11: The distribution of flight duration of debris group A, B1 and C.



Figure 12(a) shows the percentage of wind-borne debris that were initialized by the vortex at different radial positions. The percentage was calculated based on the number of debris that were initialized by the vortex at that position with respect to the total number of wind-borne debris (122, 90 and 54 debris for debris group A, B1 and C respectively). Hence, at the location  $r/r_c=1$ , 30 individual debris particles from group A were initialized yielding 24%, while 13 individual debris of debris group C were initialized yielding 24%. Figure 12(b) shows the horizontal profiles of tangential, radial and vertical velocity components that corresponds to the debris release positions. The scales of the normalized vertical velocity are shown on the left vertical axis while the normalized tangential and radial velocity are shown on the right vertical axis. This was done to highlight the distribution of vertical profile without being overshadowed by the high magnitudes of tangential velocity. As discussed earlier, the centre of the vortex primarily consists of downwards flow, while maximum magnitude of updraft flow can be found around the vortex core region,  $r/r_c=1$ . A relatively high magnitude of tangential velocity is present at the region  $r/r_c>1$ . Based on the figure, it can be observed that the percentage distribution of debris initialization based on the position shows a correlation with the vertical velocity profile. Furthermore, all three debris groups illustrate similar trends with the highest percentage at the core radius,  $r/r_c=1$  despite the difference in total number of debris considered as wind-borne. Regions further away at  $r/r_c=2.5$  and  $r/r_c=3$ , and around the centre of the vortex at  $r/r_c=0$  and  $r/r_c=0.25$  were observed to have a very low possibility of flight initiation by the flow despite the high magnitudes of tangential and radial velocities. The increase of vertical flow from  $r/r_c=0.5$  to  $r/r_c=2$  resulted in the increase in the percentage of debris initialization, where debris that were positioned around this region were approximately 10% more likely to be initialized. This is due to the upwards lift produced by the vertical velocity that provides the elevation for debris to become wind-borne. A small number of particles appear to have become windborne for debris A and B at  $r/r_c=0$ . This is due to the wandering motion of the vortex, where the core shifted approximately  $r/r_c=0.18$  from the centre axis. Although the shift is not significant, the radial outflow at the centre in addition with the absence of downward flow provided sufficient condition for debris to become wind-borne.

Figure 13 illustrates the plan view of the trajectories of all wind-borne debris for debris group A, B1, and C that were initialized from the position of  $r/r_c=0.5, 0.75, 1, 1.5$  and  $2$  to the impact on the ground surface. The positions of  $r/r_c=0, 0.25, 2.5$  and  $3$  are not shown as debris initialized from those locations was infrequent. The smaller debris (group A) were observed to have high variation in debris trajectories at all positions and the longest average flight duration. In this case, the debris were observed to circulate around the vortex core, resulting in long and scattered trajectories. On the contrary, the trajectories for the larger debris group C shows lower curvature and does not have the tendency to circulate around the vortex. In general, the distribution of trajectories for each respective debris group shows similar variation at every position.

In figure 14, the bar chart shows the distribution of impact radius while the curve (red line) corresponds to the normal distribution of all wind-borne debris, expressed in terms of the percentage of occurrence against the impact radius. The percentage was calculated based on the number of occurrences of wind-borne debris that impacted at that respective radial distance. A different range of impact radii were observed for groups A, B1 and C: debris A shows the shortest mean impact radius of  $r/r_c \sim 7.0$ , whilst debris C has the greatest impact radius of  $r/r_c \sim 9.0$ . Concurrently, debris C exhibited the highest impact potential with a maximum value of  $r/r_c \sim 12.0$ , whereas debris A and B shows comparable maximum impact radii of  $r/r_c \sim 11.0$ . The normal distribution suggests similar variation for all debris, with the standard deviation for each group  $\sim 2.0$ . Although the smaller and lighter debris A has longer flight duration, it does not impact at greater radial distance from the vortex; this phenomenon will be discussed and shown in figure 15.

Figure 15 shows the total flight duration of each individual wind-borne debris from initialization to the impact on the ground against the radial distance from the centre of the vortex throughout the flight. Thus, providing an insight to the debris trajectories in relation to the regions of the vortex whilst also characterising the behaviour of different debris groups. All debris shows a reduction in radial distance once initialized, indicating the tendency to travel towards the centre before for values of  $t_d/t_r < 0.4$ . For debris group A, the radial distance for the debris were observed to increase rapidly away from the centre after the flight time of  $t_d/t_r > 0.4$ ; while some debris were ejected outwards with the radial distance of more than  $r/r_c = 8$ , the majority of the debris circulates around the region between  $r/r_c = 6$  to 8 after the flight duration of  $t_d/t_r = 2$ . Towards the end of the flight duration, a decrease in radial distance was observed as the debris were drawn towards the vortex due to the radial inflow, as shown in figure 16.

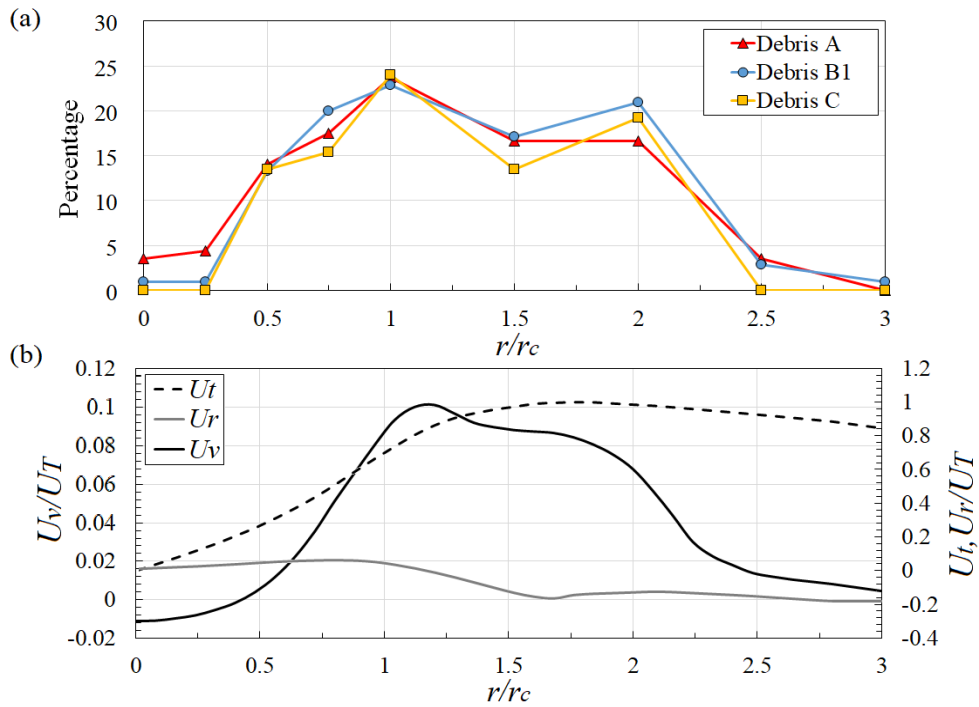


Figure 12: (a) The percentage distribution of all wind-borne debris at the position of  $r/r_c = 0, 0.25, 0.5, 0.75, 1, 1.5, 2, 2.5$  and  $3$ . (b) The horizontal profiles of tangential, radial and vertical velocities of the tornado-like vortex at the elevation of  $z/r_c = 0.015$ .

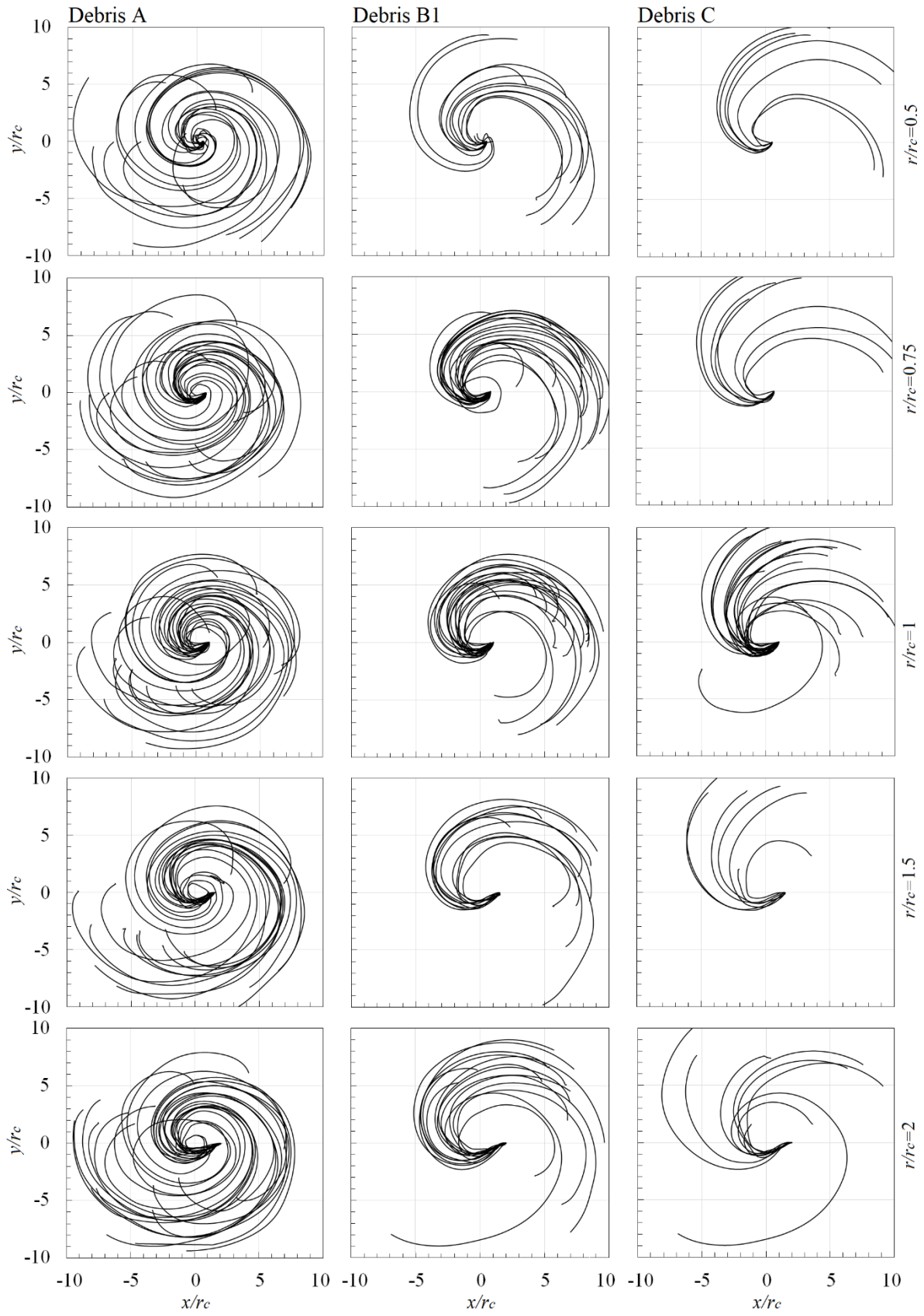


Figure 13: Plan view of debris trajectories at the locations of  $r/r_c = 0.5, 0.75, 1, 1.5$  and  $2$  for debris group A, B1 and C.

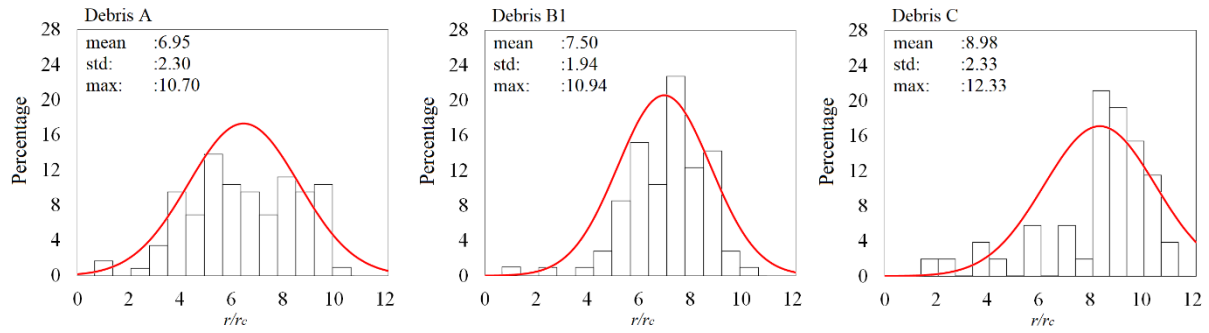


Figure 14: The distribution of impact radius of all released debris based on debris group, with mean, standard deviation and maximum values.

In general, the debris group A has approximately 60% of the flight duration around the vortex walls regions. On the contrary, the radial distance of debris group C were observed to constantly increase throughout the flight duration due to the inertia of the debris, travelling further away from the centre until the impact on the ground. The trajectories of debris group B exhibited a mixture of behaviours with some particles travelling beyond the vortex wall whilst others circulated close to walls.

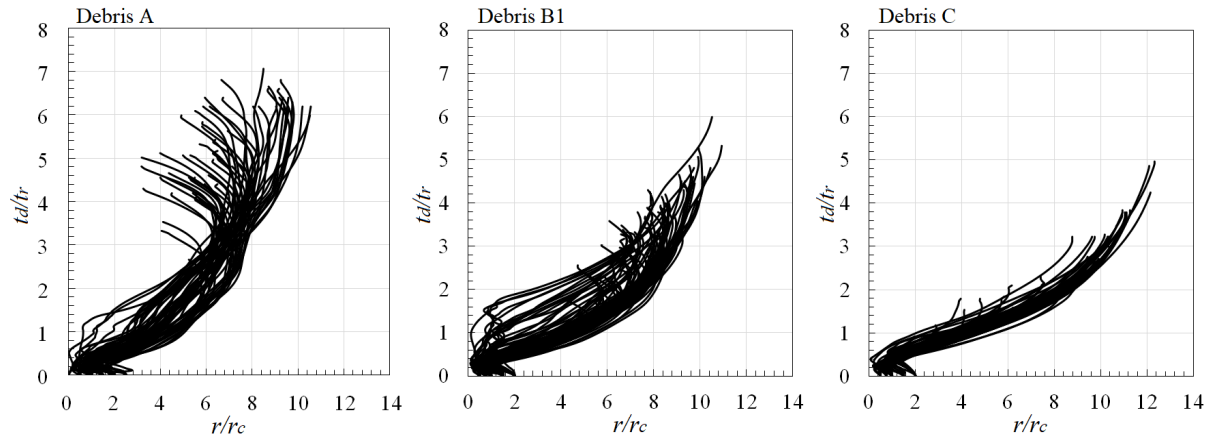


Figure 15: The flight duration of wind-borne debris against the radial distance from the centre of the vortex for debris group A, B1 and C.

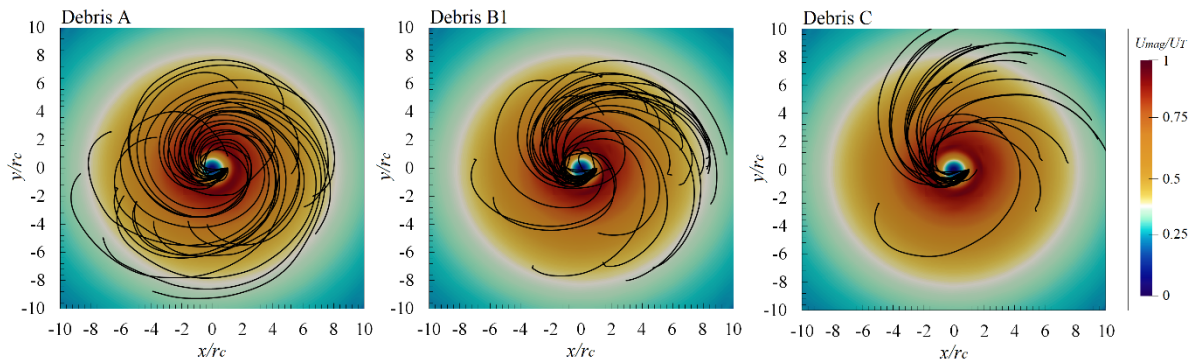


Figure 16: The top view of debris trajectories at the location  $r/r_c=1$  with the contours of averaged velocity magnitude for debris group A, B1 and C.

The plan view of the trajectories of the debris initialized from the position  $r/r_c=1$  with contours of normalized tangential velocity shown in figure 16. The red contours in figure 16 indicates the vortex walls. As discussed previously, the trajectories of debris group A are observed to circulate within the vortex wall between  $r/r_c= 1$  to 6 with a tendency to be drawn back towards the core at end of the

flight duration. However, for debris group C it is clear that the vast majority of debris are ejected away from the centre and out of the vortex walls.

## 5. CONCLUSIONS

The objective of this present research was to investigate the flight behaviour of different groups of debris in a tornado-like wind field. Hence, large eddy simulations were undertaken for a tornado-like vortex with a swirl ratio of 0.7. Acknowledging the uncertainty associated with the data, the numerical simulations agree well with previous experimental research and provide a greater insight into the flow field. The following conclusions can be made:

- The tornado-like vortex consists of two main features, a core and thick vortex wall around the core. The vortex wall consists of high velocity magnitudes where the maximum velocity components occurs around the near ground region.
- The aerodynamic behaviour for three groups with the same Tachikawa number (B1, B2 and B3) shows very similar flight behaviour and trajectories. All three debris groups exhibit a mean flight duration of  $t_d/t_r \approx 4$  with an impact radius of  $r/r_c \sim 7.5$ .
- The aerodynamic behaviour for three groups with varying Tachikawa numbers (A, B1 and C) demonstrated that debris group with a lower mass (A) has the highest percentage of wind-borne particles (~27%) compared to 20% and 12% for debris group B1 and C respectively. Group A also had a considerably longer flight duration ( $t_d/t_r \sim 6.0$ ), than groups B and C with  $t_d/t_r \sim 4.0$  and  $3.0$  respectively. During debris initializing stage, the debris positioned at the radial location of  $r/r_c=1$  had the highest possibility of becoming wind-borne, whereas debris positioned around the regions within the core at  $r/r_c=0$  and  $0.25$  and at regions where  $r/r_c > 2.0$  were less likely to be initialized. This was due to the higher vertical velocities around  $r/r_c = 1$  which appear to be key to flight initiation.
- The distribution of trajectories for debris group A were found to be scattered with high variation but low average impact range of  $r/r_c = 7.0$ , whilst debris group C has trajectories with a lower curvature but greater high radius ( $r/r_c \sim 9.0$ ). Further analysis of the flight duration indicated that debris group A had the tendency to circulate within the regions of vortex walls with consistent radial distance from the centre, whereas for group C the radial distance was observed to constantly increase until the particles impacted on the ground.
- Low mass debris with high values of  $K$  were prone to travel for longer flight duration but as indicated above, tended to be trapped within the vortex walls. This has important implications when considering the wind loading arising from wind borne debris as a result of tornadic activity.

The flow field of the tornado-like vortex and the flight behaviour of different debris groups were discussed in detail. It is worth noting that current study only considers the flow field of the vortex at  $S=0.7$ . Different swirl ratios have the potential to result in different flow characteristics and those would affect the overall behaviour of wind-borne trajectory. Further, the flight characteristics of debris were assumed with no rotation, which might be considered less realistic in a highly swirling vortex flow field when the rotation of debris generates lift, which would lead to a different interaction between the fluid and debris. It is also worth noting that this work has simulated the flow assuming one single definition of aspect ratio, but as indicated by Gillmeier et al. (2019) and Gairola and Bitsuamlak (2019), this may be an important area which has hitherto largely been neglected. Notwithstanding this, this research shows the flight behaviour of different debris groups and their corresponding impact range and thus enables the potential dangers associated with flying debris in tornadoes to be evaluated.

## Acknowledgements

The authors would like to acknowledge the Birmingham Environment for Academic Research (BlueBEAR) at the University of Birmingham for providing the software licenses and computational resources.

## Reference

- [1]. Alexander, C.R., Wurman, J., 2005. The 30 May 1998 Spencer, South Dakota, Storm. Part I: The Structural Evolution and Environment of the Tornadoes,” AMS Monthly Weather Review, v. 133, 72-96.
- [2]. Baker, C. J., 2007. The debris flight equations. Journal of Wind Engineering and Industrial Aerodynamics 95(5):329-353.
- [3]. Baker, C.J., Sterling, M., 2017. Modelling wind fields and debris flight in tornadoes, J. Wind Eng. and Ind. Aerody., 168, 312-321.
- [4]. Bourriez, F., Sterling, M., Baker, C.J., 2017. Physically modelling windborne debris in tornado-like flow, 9<sup>th</sup> Asia-Pacific Conference on Wind Engineering, Auckland, New Zealand, 2017.
- [5]. Courant, R., Friedrichs, K., Lewy, H., 1928. Über die partiellen Differenzengleichungen der mathematischen Physik, Mathematische Annalen (in German), 100 (1): 32–74.
- [6]. Darrow, M., 2019. Day 4-8 Severe Weather Outlook Issued on Feb 28, 2019. Norman, Oklahoma: Storm Prediction Center. Retrieved from [https://www.spc.noaa.gov/products/exper/day4-8/archive/2019/day4-8\\_20190228.html](https://www.spc.noaa.gov/products/exper/day4-8/archive/2019/day4-8_20190228.html)
- [7]. English, E. C., Holmes, J. D., 2005. Non-dimensional solutions for trajectories of wind-driven compact ob-jects, Proceedings of The Fourth European and African Conference on Wind Engineering.
- [8]. Evans, S., 2019. U.S. Severe weather in May to drive \$2 Billion or greater financial impact on: AON. Retrieved from <https://www.artemis.bm/news/u-s-severe-weather-in-may-to-drive-2bn-or-greater-financial-impact-aon/>
- [9]. Gairola, A., Bitsuamlak, G., 2019. Numerical tornado modelling for common interpretation of experimental simulators. Journal of Wind Engineering and Industrial Aerodynamics, Volume 186, pages 32-48.
- [10]. Gillmeier, S., Hemida, H. and Sterling, M., 2016. An analysis of the influence of a tornado generators geometry on the flow field. 8th International Colloquium on Bluff Body Aerodynamics and Applications June 7 – 11.
- [11]. Gillmeier, S., Sterling, M., Baker, C.J. and Hemida, H., 2017. A reflection on analytical vortex models used to model tornado-like flow fields. International Workshop on Physical Modelling of Flow and Dispersion Phenomena Dynamics of Urban and Coastal Atmosphere.
- [12]. Gillmeier, S., Sterling, M., and Hemida, H (2019). Simulating Tornado-Like Flows – the Effect of the Simulator’s Geometry. Meccanica. Vol. 54, No. 15, 2385-2398, <https://doi.org/10.1007/s11012-019-01082-4>.
- [13]. Hangan, H. and Kim, J.D., 2006. Numerical simulation of Tornado Vortices. The 4th International Symposium on Computational Wind Engineering, Yokohama.
- [14]. Hangan, H. and Kim, J.D., 2008. Swirl ratio effects on tornado vortices in relation to the Fujita scale. Wind Struct. 11, 291–302.
- [15]. Harms, Associate Writer Nicole. (2019, February 17). Why Are Tornadoes So Terrifying? Retrieved from <https://www.thoughtco.com/tornado-safety-overview-3444293>
- [16]. Holmes, J. D., Baker, C. J., Tamura, Y., 2006. Short note Tachikawa number: A proposal, Journal of Wind Engineering and Industrial Aerodynamics 94, 41-47.

- [17].Holmes, J. D., 2004. Trajectories of spheres in strong winds with application to wind-borne debris, *Journal of Wind Engineering and Industrial Aerodynamics* 92, 9-22.
- [18].Holmes, J. D., English, E. C., Letchford, C., 2004. Aerodynamic forces and moments on cubes and flat plates, with applications to wind-borne debris, *Summary Papers of the 5th International Colloquium on Bluff Body Aerodynamics and Applications*, 103-106.
- [19].Howells, P.C., Rotunno, R., Smith, R.R., 1988. A comparative study of atmospheric and laboratory analogue numerical tornado-vortex models. *Quarterly Journal of Royal Meteorological Society* 114, 801–822
- [20].ICEM, C., 2012. ver. 14.0. ANSYS Inc., Southpointe, 275.
- [21].Ishihara, T. and Liu, Z.Q., 2014. Numerical study on dynamics of a tornado-like vortex with touching down by using the LES turbulence model. *Wind and Structures*, Vol, 19, No. 1 000-000.
- [22].Ishihara, T., Oh, S. and Tokuyama, Y., 2011. Numerical study on flow fields of tornado-like vortices using the LES turbulence model. *Journal of Wind engineering and Industrial Aerodynamics* 99, 239–248.
- [23].Kosiba, K. A., Robinson, P., Chan, P. W., & Wurman, J. (2014). Wind Field of a Non mesocyclone Anti cyclonic Tornado Crossing the Hong Kong International Airport. *Advances in Meteorology*, 1-7.
- [24].Kuai, L., Haan, F.L., Gallus, W.A. and Sarkar, P.P., 2008. CFD simulations of the flow field of a laboratory-simulated tornado for parameter sensitivity studies and comparison with field measurements. *Wind and Structures*. 11, 1-22.
- [25].Kuai, L., Haan, F.L., Gallus, W.A. and Sarkar, P.P., 2008. CFD simulations of the flow field of a laboratory-simulated tornado for parameter sensitivity studies and comparison with field measurements. *Wind and Structures*. 11, 1-22.
- [26].Lewellen, D.C., Lewellen, W.S., 2007. Near-surface intensification of tornado vortices. *Journal of the Atmospheric Sciences* 64, 2176–2194.
- [27].Lewellen, D.C., Lewellen, W.S., Xia, J., 1999. The influence of a local swirl ratio on tornado intensification near the surface. *Journal of the Atmospheric Sciences* 57, 527–544.
- [28].Lin, N., Holms J. D., Letchford, C. W., 2007. Trajectory of windborne debris and applications to impact test-ing, *J. Structural Eng. ASCE*, 133(2), 274-282.
- [29].Liu, Z, Ishihara, T., 2015. Numerical study of turbulent flow fields and the similarity of tornado vortices using large eddy simulations. *Journal of Wind engineering and industrial aerodynamics*. 145, 42-60.
- [30].Maruyama, T., 2009. A Numerically Generated Tornado-like Vortex by Large Eddy Simulation, *Proceedings of Seventh Asia-Pacific Conference on Wind Engineering*, Taipei Taiwan, 2009.8, pp. 349-352.
- [31].Maruyama, T., 2011. Simulation of flying debris using a numerically generated tornado-like vortex. *J. Wind Eng. Ind. Aerod.* 99, 249–256.
- [32].Maas H-G, Gruen A., Papantoniou D., 1993. Particle tracking velocimetry in three-dimensional flows. Part I. *Exp Fluid*, 15:133–46.
- [33].Malik N.A., Dracos T., Papantoniou D., 1993. Particle tracking velocimetry in three-dimensional flows. Part II. *Exp Fluid*, 15:279–94.
- [34].Matsui, M., Tamura, Y., Yoshida, A., 2008. Wind pressure distribution around cube in tornadic flow and moving effects on tornadic flow, *Proc. 20th National Symposium on Wind Engineering*, pp.319-324 (Japanese).
- [35].Matsui, M., Tamura,Y., 2009. Influence of swirl ratio and incident flow conditions on generation of tornado-like vortex. In: *Proceedings of the 5<sup>th</sup> European and African Conference on Wind Engineering*. CD-ROM.



- [36]. Mitsuta, Y., Monji, N., 1984. Development of a laboratory simulator for small scale atmospheric vortices. *Nat. Disaster Sci.* 6, 43–54.
- [37]. Monji, N., 1985. A laboratory investigation of the structure of multiple vortices. *J. Meteorol. Soc. Jpn.* 63, 703–712.
- [38]. Natarajan, D., 2011. Numerical Simulation of Tornado-like Vortices. (Unpublished doctoral thesis). University of Western Ontario, Canada.
- [39]. Nolan, D.S., Farrell, B.F., 1999. The structure and dynamics of tornado-like vortices. *Journal of the Atmospheric Sciences* 56, 2908–2936.
- [40]. OpenFOAM, 2019. OpenFOAM: User guide version 7. Retrieved from <http://foam.sourceforge.net/docs/Guides-a4/OpenFOAMUserGuide-A4.pdf>
- [41]. Phuc, P.V., Nozu, T., Nozawa, K., Kikuchi, H., 2012. A Numerical Study of the Effects of Moving Tornado-Like Vortex on a Cube. The Seventh International Colloquium on Bluff Body Aerodynamics and Applications (BBAA7) Shanghai, China; September 2-6, 2012.
- [42]. Putnam, A., 1961. Integrable form of droplet drag coefficient, *ARS Jnl.*, 31, 1467.
- [43]. Smagorinsky, J., 1963. General Circulation Experiments with the Primitive Equations. *Monthly Weather Review.* 91 (3): 99–164.
- [44]. Refan, Maryam & Hangan, Horia. (2018). Near surface experimental exploration of tornado vortices. *Journal of Wind Engineering and Industrial Aerodynamics.* 175C.
- [45]. Richards, P.J., Williams, N., Laing, B., McCarty, M., Pond, M., 2008. Numerical calculation of the 3-dimensional motion of wind-borne debris, *J. Wind Eng. and Ind. Aerody.*, 96, 2188-2202.
- [46]. Tachikawa, M., 1983. Trajectories of flat plates in uniform flow with application to wind-generated missiles, *Journal of Wind Engineering and Industrial Aerodynamics* 14, 443-453.
- [47]. Tang, Z., Feng, C., Wu, L., Zuo, D., James, D.L. (2018) "Characteristics of tornado-like vortices simulated in a large-scale wind-tunnel simulator." *Boundary-Layer Meteorology*, 166, 327-350.
- [48]. Tari, P.H., Gurka, R., Hangan, H., 2010. Experimental investigation of tornado-like Vortex dynamics with swirl ratio: the mean and turbulent flow fields. *J. Wind Eng. Ind. Aerodyn.* 98, 936–944.
- [49]. Van Driest, E.R., 1956. Turbulent flow near a wall, *J. Aeronaut. Sci.*, 23, No. 11, 1007-1011.
- [50]. Wang, K. and Letchford, C. W., 2003. Flying debris behaviour, 11th International Conference on Wind Engineering, Lubbock, Texas Proceedings 2, 1663-1670.
- [51]. Ward, N. B., 1972. The exploration of certain features of tornado dynamics using a laboratory model. *J. Atmos. Sci.*, 29, 1194-1204.
- [52]. Watkins, S., Mousley, P.D., Hooper, J.D., 2002. Measurement of fluctuating flows using multi-hole probes. Proceedings of the 9th International Congress of Sound and Vibration, Orlando, Florida, USA, 8-11 July, International Institute of Acoustics and Vibration (IIAV).
- [53]. Wilson, T., Rotunno, R., 1986. Numerical simulation of a laminar end-wall vortex and boundary layer. *Phys. Fluids* 29, 3993–4005.
- [54]. Wills, J. A. B., Lee, B. E., and Wyatt, T. A., 2002. A model of wind-borne debris damage, *Journal of Wind Engineering and Industrial Aerodynamics* 90, 555-565.
- [55]. Yang, Z., 2015 Large-eddy simulation: Past, Present and the future. *Chinese Journal of Aeronautics*, (2015), 28 (1): 11-24.